Available online at www.sciencedirect.com
ScienceDirect
International Journal of Multiphase Flow 32 (2006) 1269–1286
International Journal of Multiphase Flow
www.elsevier.com/locate/ijmulflow

On the departure behaviors of bubble at nucleate pool boiling

Jeongbae Kim [a], Moo Hwan Kim [b,*]

[a] Renewable Energy Research Department, KIER (Korea Institute of Energy Research), 71-2, Jang-dong, Yuseong-gu, Daejeon 305-343, Republic of Korea
[b] Department of Mechanical Engineering, Pohang University of Science and Technology, San 31, Hyoja-dong, Namgu, Pohang, Kyoungbuk 790-784, Republic of Korea

Received 26 June 2005; received in revised form 8 June 2006

Abstract

Dimensionless scales of radius and time, proposed by the authors in a previous study, were used to quantitatively analyze the bubble departure radius and time during nucleate pool boiling. The results obtained from dimensional analysis were compared with experimental data reported in many studies. These experimental data are including partial nucleate pool boiling data with constant heat flux and temperature conditions acquired over the past 40 years at atmospheric and sub-atmospheric pressures, as well as data obtained at subcooled, saturated, and superheated pool temperature conditions.

It was shown that the departure radius and time could be well correlated with respect to Jakob number as proposed by the previous studies. And the bubble departure behaviors well categorized between atmospheric and sub-atmospheric pressure, which is occurred from the different growth rate near the departure time partial nucleate pool boiling.

For almost all obtained under atmospheric pressure, the dimensionless departure radius and time scales were about 25 and 60, respectively. For higher Jakob number, the square root of Bond number was proportional to the power of 0.7 of Jakob number, little different from the previous correlations. The dimensional departure radius and time estimated from the relationships proposed in this study were compared with measured departure scales and the results obtained with the previous correlations. And it was shown that the relationships could well predict and describe the departure behaviors of bubble during nucleate pool boiling.

Keywords: Bubble departure radius; Bubble departure time; Nucleate pool boiling; Bond number; Jakob number

1. Introduction

The complete process of liquid heating, nucleation, bubble growth, and departure is the central mechanism of two-phase heat transfer from a superheated wall during nucleate pool boiling. Two features of this process that affect the rate of heat transfer during the ebullition cycle are the bubble radius at departure, R_d, and the frequency at which bubbles are generated and departed, f.

* Corresponding author. Tel.: +82 54 279 2165; fax: +82 54 279 3199.
E-mail address: mhkim@postech.ac.kr (M.H. Kim).

0301-9322/$ - see front matter © 2006 Elsevier Ltd. All rights reserved.
doi:10.1016/j.ijmultiphaseflow.2006.06.010

Since the bubble radius and frequency of departure must be related, the departure radius and the bubble growth rate must be also related. The inverse of the frequency, $\tau = 1/f$, which is the time period associated with the growth of each bubble, must equal the sum of the waiting period and the time required for the bubble to grow to its departure radius:

$$\frac{1}{f} = \tau = t_w + t_d \tag{1}$$

where, t_w is the waiting period and t_d is the departure time.

Therefore, the frequency of bubble departure depends directly on how large the bubble must become in order for it to depart, and, as a consequence, on the growth rate at which the bubble can grow to this size on the heating surface.

The bubble radius at departure is primarily determined by the net effect of forces acting on the bubble as it grows on the surface. Interfacial tension acting along the contact line invariably acts to hold the bubble in place on the surface. Buoyancy is often a major player in the force balance, although its effect depends on the orientation of the surface with respect to the accelerating or gravitational body force vector.

If the bubble growth rate is high, the inertia associated with the induced liquid flow field around the bubble may also tend to pull the bubble away from the surface. When the liquid adjacent to the surface has a bulk motion associated with it, drag and lift forces on the growing bubble may also act to detach the bubble from the surface. In addition, because the rate of bubble growth and the shape of the bubble (hemispherical or spherical) may affect the conditions for bubble departure, the departure radius may be affected by the wall superheat, the contact angle, θ, and the thermodynamic properties of the liquid and vapor phases.

The departure radius of the bubble during nucleate boiling has been the subject of numerous investigations. In experimental studies, the departure radius has typically been determined from high-speed movies of the boiling process. Based on data obtained in this manner, a number of investigators have proposed correlation equations that may be used to predict the departure radius of bubbles during nucleate boiling.

Many of the correlations are written in terms of the Bond number, Bo, defined as

$$Bo = \frac{g(\rho_l - \rho_v)(2R_d)^2}{\sigma} \tag{2}$$

where, g is gravity, ρ_l is the liquid density, ρ_v is the vapor density, and σ is the liquid surface tension.

This same dimensionless group is also sometimes referred to as the Eotvos number.

Cole and Shulman (1966b) proposed a relation in which $Bo^{1/2}$ is simply proportional to the inverse of the absolute pressure,

$$Bo^{1/2} = \frac{1000}{P} \tag{3}$$

where, P is the pressure in mmHg.

This relation contrasts sharply with other relations where the dimensionless departure diameter $Bo^{1/2}$ depends on a complex combination of physical properties. The success of Eq. (3) is apparently a result of the fact that $1000/P$ approximates the combined pressure dependence of the properties that appear in the other relations. In a subsequent study, Cole (1967) proposed

$$Bo^{1/2} = 0.04\, Ja \tag{4}$$

This relation is an extension of Eq. (3) in the sense that the pressure term is taken into account by the inclusion of the vapor density in the Jakob number, Ja, defined as $Ja = \rho_l C_{pl} \Delta T / \rho_v h_{fg}$, based on the temperature difference between the wall and the saturation. In the Jakob number, C_{pl} is the liquid specific heat, $\Delta T (= T_{wall} - T_{sat})$ is the wall superheat, h_{fg} is the latent heat, T_{wall} is the wall temperature, and T_{sat} is the saturation temperature.

Later, Cole and Rohsenow (1968) proposed a new relation as an evolutionary improvement of Eq. (4),

$$Bo^{1/2} = C\, Ja^{c^{5/4}} \tag{5}$$

where $C = 1.5 \times 10^{-4}$ for water, $C = 4.65 \times 10^{-4}$ for fluids other than water.

In Eq. (5), the wall superheat was replaced by the critical temperature, T_c, because experimental data contradicted the proportionality between the wall superheat and departure radius implied by Eq. (4). Therefore, the Jakob number was described as

$$Ja^c = \frac{\rho_l C_{pl} T_c}{\rho_v h_{fg}} \tag{6}$$

Golorin et al. (1978) later developed the following correlation:

$$\frac{2R_d}{d_1} = 1 + \frac{d_2}{d_1} \tag{7}$$

$$d_1 = \frac{1.65 d^* \sigma}{g(\rho_l - \rho_v)} \tag{8}$$

$$d_2 = \left[\frac{15.6\rho_l}{g(\rho_l - \rho_v)}\right]^{1/3} \left[\frac{\beta_d k_l (T_{wall} - T_{sat})}{\rho_v h_{fg}}\right]^{2/3} \tag{9}$$

where, k_l is the liquid conductivity, $d^* = 6.0 \times 10^{-3}$ mm, $\beta_d = 6.0$ for water, alcohol, and benzene.

This correlation includes the dynamic interaction between the growing bubble and the surrounding liquid, as well as the small-scale roughness of the heating surface. Kutateladze and Gogonin (1979) found that they could correlate a large body of data from the literature using

$$Bo^{1/2} = 0.25(1 + 10^5 K_1)^{1/2} \quad \text{for } K_1 < 0.06 \tag{10}$$

$$K_1 = \left(\frac{Ja}{Pr_l}\right) \left\{ \left[\frac{g\rho_l(\rho_l - \rho_v)}{\mu_l^2}\right] \left[\frac{\sigma}{g(\rho_l - \rho_v)}\right]^{3/2} \right\}^{-1} \tag{11}$$

where, Pr_l is liquid Prandtl number and μ_l is the liquid viscosity.

This correlation contains only the Bond number and the dimensionless group K_1.

Jensen and Memmel (1986) recently compared the above correlations against available departure radius data and proposed an improvement to the Kutateladze and Gogonin (1979) correlation,

$$Bo^{1/2} = 0.19(1.8 + 10^5 K_1)^{2/3} \tag{12}$$

Although different cavities will generate bubbles at different frequencies, it can be useful to consider the mean bubbling frequency, f, associated with the boiling process for a given solid liquid combination and imposed conditions. Peebles and Garber (1953) proposed the relation

$$f(2R_d) = 1.18 \left[\frac{t_d}{t_d + t_w}\right] \left[\frac{\sigma g(\rho_l - \rho_v)}{\rho_l^2}\right]^{1/4} \tag{13}$$

Other correlations proposed in previous studies can be found in Table 1. All correlations described in this study were obtained from Carey (1992).

However, previous studies usually used the results obtained when the bubble departed from the heating surface with a constant heat flux condition, while we used experimental results recently obtained with constant temperature conditions and analyzed the characteristics when the bubble departed from the heating surface using the dimensionless characteristic radius and time proposed by Lee et al. (2003). The Jakob number considered in this study ranged from 15 to 2100. When $Ja < 30$, the experiments were performed in the partial nucleate boiling region at atmospheric pressure conditions. When $Ja > 30$ except for one data, the experiments were performed at sub-atmospheric pressure conditions. The working fluids included binary mixtures as well as pure substances.

For atmospheric and saturated pool conditions, we used the results of Staniszewski (1959), Han and Griffith (1965), and Fontana (1972) for water, Cole and Shulman (1966a) for *n*-pentane, Lee et al. (2003) and Kim et al. (2004) for R11 and R113, and Lee et al. (2004) for binary mixtures consisting of R11 and R113. For atmospheric and other pool temperatures, we used Zuber (1961) for water and subcooled conditions, Kim et al. (2002) for FC-72 and subcooled conditions, and Kim et al. (2004) for R113 and subcooled, saturated, and superheated pool conditions. The experiments of Lee et al. (2003, 2004) and Kim et al. (2004)

Table 1
Departure radius and frequency correlations

$Bo^{1/2} = 0.0208\theta$ where θ is the contact angle in degrees	Fritz (1935)
$Bo^{1/2} = \left[\frac{\sigma}{g(\rho_l - \rho_v)}\right]^{-1/6}\left[\frac{6k_l(T_{wall} - T_{sat})}{q''}\right]^{1/3}$	Zuber (1959)
$Bo^{1/2} = \left[\frac{3\pi^2\rho_l^2\alpha_l^2 g^{1/2}(\rho_l - \rho_v)^{1/2}}{\sigma^{3/2}}\right]^{1/3} Ja^{4/3}$	Ruckenstein (1963)
$\frac{R_d}{R_F} = -\frac{C}{2R_F} + \sqrt{\frac{C^2}{(2R_F)^2} + 1}$ where R_F is the radius with Fritz (1935)	Borinshansky and Fokin (1963)
$C = \left(\frac{6}{g}\right)\left(\frac{\rho_l}{\rho_l - \rho_v}\right)\left(\frac{\rho_v}{\rho_l}\right)^{0.4}\left[\frac{q''}{\rho_v h_{fg}}\right]$	
$Bo^{1/2} = \frac{1000}{P}$ where P is pressure in mmHg	Cole and Shulman (1966)
$f(2R_d) = 0.078$	Jakob and Fritz (1931)
$f(2R_d) = 0.59\left[\frac{\sigma g(\rho_l - \rho_v)}{\rho_l^2}\right]^{1/4}$	Zuber (1963)
$f^2(2R_d) = \text{constant}$ for dynamically (inertia) controlled growth	Ivey (1967)
$f^{1/2}(2R_d) = \text{constant}$ for thermally (heat transfer) controlled growth	
$f^2(2R_d) = \frac{4}{3}\frac{g(\rho_l - \rho_v)}{C_d\rho_l}$ where C_d is a bubble drag coefficient, $C_d = 1$ for water at 1 atm	Cole (1960)
$f^{1/2}(2R_d) = \frac{4}{\pi}Ja\sqrt{3\pi\alpha_l}\left\{\left(\frac{t_d}{t_d + t_w}\right)^{1/2} + \left(1 + \frac{t_d}{t_d + t_w}\right)^{1/2} - 1\right\}$	Mikic and Rohsenow (1969)
$f^{1/2}(2R_d) = 0.83Ja\sqrt{\pi\alpha_l}$ for $0.15 < t_d/(t_d + t_w) < 0.8$	

Table 2
Experimental conditions used to obtain the data referred to in this study

Pressure	Heating surface	Fluid	Subcooled	Saturated	Superheated
Atmospheric	Constant heat flux	Water	Zuber (1961), #1	Staniszewski (1959), #1 Han and Griffith (1965), #1 Fontana (1972), #1	
		n-Pentane		Cole and Shulman (1966a), #1	
	Constant temperature	R11		Lee et al. (2003), #4	
		R113	Kim et al. (2004), #14	Lee et al. (2003), #1 Kim et al. (2004), #1	Kim et al. (2004), #2
		Binary: R11 + R113		Lee et al. (2004), #4	
		FC-72	Kim et al. (2002), #1		
Sub-atmospheric	Constant heat flux	Water		Cole and Shulman (1966a), #4 van Stralen et al. (1975), #5	
		Methanol		Cole and Shulman (1966a), #3	
		n-Pentane		Cole and Shulman (1966a), #1	

were performed at constant temperature conditions. Finally, for sub-atmospheric and almost nearly saturated conditions, we used Cole and Shulman (1966a) for methanol, water, and *n*-pentane, and van Stralen et al. (1975) for water. The experimental conditions are clearly indicated in Table 2, and the sets of data will be referred to using the numbers indicated in the table.

2. Experiments

2.1. Experimental apparatus

The experimental data for constant temperature conditions were mainly obtained from previous studies by the authors. In these studies, we used a microscale heater array to maintain a constant temperature at

the heating surface and to measure the heat flow rate. The heater was fabricated on a transparent glass wafer using a very-large-scale-integrated (VLSI) technique. The transparency provided a bottom view of the growing bubble, which was captured using a high-speed CCD camera. First, a titanium and platinum layer for the heater line on the wafer was installed using thermal evaporation. Then, a titanium and platinum layer for the power line was fabricated. The roughness of the heating surface was approximately 0.4 μm, which was the height of the heating line with respect to the base substrate. The static contact angle of the microscale heater array surface was 71° for distilled water and 11.4° for R113, which indicates the hydrophilic nature of R113. A total of 96 microscale heaters comprised one microscale heater array. Each microscale heater measured 0.27×0.27^{2}, and the total size of the microscale heater array was $2.7 \times 2.7\ m^2$. For our experiments, the heater was manufactured at the Samsung Advanced Institute of Technology based on the idea of Rule et al. (1998) and Rule and Kim (1999). Most of the experimental devices that have been used previously to control the power of the heating block beneath the bubble, and thereby provide a constant heat flux, could not maintain a constant surface temperature over very short time intervals. However, our microscale heater array was controlled with a Wheatstone bridge circuit that provided a constant surface temperature with a high temporal resolution. The longest time delay in the circuit occurred at the OP amp, which had a time resolution of 10^{-7} s Due to the fast response of the circuitry, good repeatability was achieved in our experimental results.

To maintain and control the constant temperature conditions, each heater was previously calibrated for temperatures ranging from 20 to 80 °C. The temperature of the 96 heaters in the array was controlled by 96 electric Wheatstone bridge feedback circuits, which were operated in a manner similar to that used for constant-temperature hot-wire anemometry. Each heater in the array could be represented as one resistor in a Wheatstone bridge circuit. The detail calibration process for the wall temperature of the heater was described in Lee et al. (2003). A data acquisition system that could measure and store data at 7.35 kHz with 12-bit resolution was used to measure the heat flow rate of each heater throughout the experiments. Therefore, the voltage data for each heater were sampled every 0.136 ms and 1000 voltage readings for each heater were stored with 12-bit resolution. All the tests performed in this study lasts 136 ms. These measurements were synchronized with the images captured by the high-speed CCD camera. A more detail description can be found in Rule and Kim (1999). Fig. 1 shows a schematic diagram of the experimental apparatus. Ten thin film heaters with 15,500 W/m^2 were used to control the liquid temperature inside the test chamber without providing another heat source for the bubble. A 150-W cold light source was used for the CCD camera. The maximum speed of CCD camera (Redlake Co., HG-100K) was 100,000 frames per second. A long distance microscopic lens was used to capture the small bubbles during boiling (see Fig. 1).

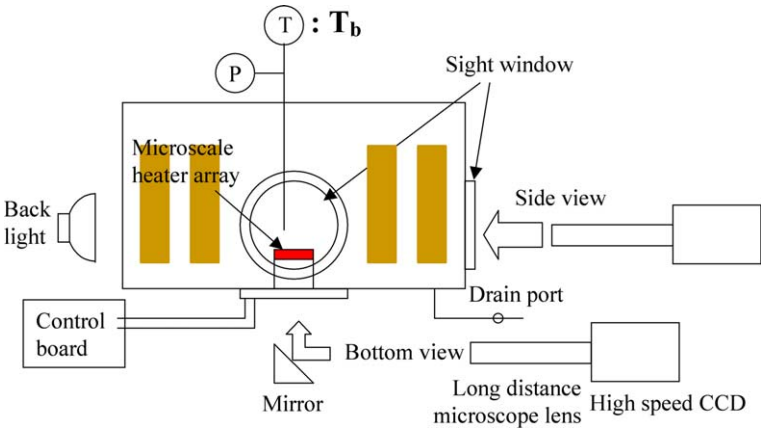

Fig. 1. Schematic diagram of the experimental apparatus.

2.2. Uncertainty analysis

The bubble growth behavior was analyzed using side-view images, while the heat flow rate was measured using the microscale heater during growth. Since most previous results for bubble growth have been for a spherical bubble, the growth behavior in this study was analyzed using the equivalent radius of a sphere with the same volume. The images captured from inception to departure showed reasonable bubble geometries, with an axi-symmetric shape about the vertical axis and a non-symmetric shape about the horizontal axis, as shown like Fig. 2. Based on the shape assumption, we calculated the volume of the upper and lower parts of the bubble using

$$V_{\mathrm{U}} = \frac{2}{3}\pi B^2 A \tag{14}$$

$$V_{\mathrm{L}} = \pi B^2 \left[D - \frac{D^3}{3E^2} \right], \quad E = \sqrt{\frac{D^2}{1 - \frac{(C/2)^2}{B^2}}} \tag{15}$$

where, A, B, C, D and E are the dimensions indicated in Fig. 2. V_{U} is the volume of the upper part of the bubble, and V_{L} is the volume of the lower part of the bubble. V_{L} can also be calculated using B, D, and C (see Fig. 2).

The equivalent radius, R, can then be defined as the radius for which the total volume (V) from the measurements is balanced with that of a sphere with an equivalent radius,

$$V = V_{\mathrm{U}} + V_{\mathrm{L}} = \frac{4}{3}\pi R_{\mathrm{eq}}^3 \tag{16}$$

$$R = \left(\frac{1}{2} B^2 A + \frac{3}{4} B^2 \left[D - \frac{D^3}{3E^2} \right] \right)^{\frac{1}{3}} \tag{17}$$

The equivalent radius can be calculated from the dimensions shown in Fig. 2; however, the errors in the dimensional measurements will propagate into the calculation of the equivalent radius. The dimensions shown in Fig. 2 were measured by counting the number of pixels in each captured image. A micrometer was placed in the chamber at the same distance as the bubble nucleation to provide guidance for the size measurements. From the captured micrometer images, a physical dimension of 1000 mm corresponded to 197 pixels in our experiments. Therefore, one pixel in each image corresponded to 5.0761 μm. The clearly captured images could be measured with an error of ±1 pixel. An uncertainty analysis was performed using the method described by Coleman and Steele (1989). The maximum uncertainty in the first image, which contained the smallest bubble, was 5.0%.

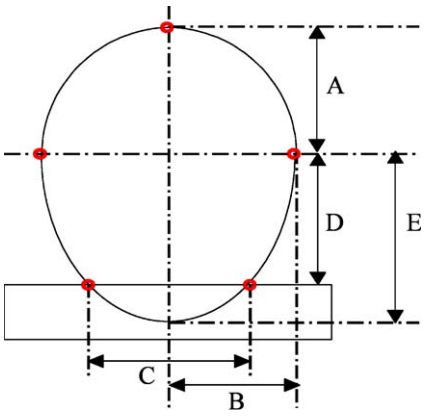

Fig. 2. Geometry of the spheroid used to determine the bubble volume.

Lee et al. (2003) captured bubble images with a time resolution of 1.0 ms (1000 frames/s), while Lee et al. (2004) captured bubble images with a time resolution of 0.25 ms (4000 frames/s). Kim et al. (2004) captured bubble images with a time resolution of 0.2 ms (5000 frames/s).

3. Results and discussion

3.1. Dimensional analysis of the bubble growth and departure

We performed a dimensional analysis to compare the growth and departure behavior with the same scales, which required the characteristic time and length scales.

Suppose that the bubble growth can be characterized by the pressure difference (ΔP) between the vapor and the bulk liquid pressures. Then, the characteristic velocity scale (v_c) may be determined from the driving potential,

$$v_c = \frac{R_c}{t_c} = \sqrt{\frac{2}{3}\frac{\Delta P}{\rho_l}} \tag{18}$$

where, R_c is the characteristics bubble radius scale, t_c is the characteristics time scale.

Here, the factor of two-thirds was inserted to allow comparisons with the dimensionless parameter of Mikic et al. (1970).

The characteristic time scale can be determined from the ratio of the corresponding latent heat transfer and the conduction heat transfer rate through the interface,

$$\frac{q_{\text{latent}}}{\dot{q}_{\text{conduction}}} = \frac{\rho_v h_{fg}\frac{4}{3}\pi R^3}{k_l 4\pi R^2 \frac{\partial T}{\partial r}} = \frac{1}{3}\frac{\rho_v h_{fg} R_c^3}{k_l R_c^2}\frac{T_c}{R_c}\frac{R^{+3}}{R^{+2}\frac{\partial T^+}{\partial r^+}} = t_c \frac{R^+}{\frac{\partial T^+}{\partial r^+}} \tag{19}$$

$$t_c = \frac{1}{3}\frac{\rho_v h_{fg} R_c^2}{k_l T_c} = \frac{1}{3}\frac{\rho_v h_{fg} R_c^2}{k_l \Delta T} = \frac{1}{3}\frac{1}{Ja\alpha}R_c^2 \tag{20}$$

where k_l is the thermal conductivity, T is the temperature, and α is the thermal diffusivity of the liquid.

If the bulk liquid is saturated, bubble growth should be influenced by the wall superheat. The Jakob number is defined by $(\rho_l C_{P_l}\Delta T)/(\rho_v h_{fg})$, where the wall superheat ($\Delta T = T_{wall} - T_{sat}$) is used as the characteristic temperature scale ($T_c = \Delta T = T_{wall} - T_{sat}$). From Eqs. (18) and (20), the characteristic radius and time scales are

$$R_c = \sqrt{\frac{27}{2}}Ja\alpha\sqrt{\frac{\rho_l}{\Delta P}}, \quad t_c = \frac{9}{2}Ja\alpha\frac{\rho_l}{\Delta P} \tag{21}$$

We will use the departing radius as a scaling parameter to adjust for the thermal growth behavior near the departing time. Mikic et al. (1970) assumed that bubble motion was governed by the extended Rayleigh equation,

$$\Delta P = P_v - P_\infty = \rho_l R\frac{d^2R}{dt^2} + \frac{3}{2}\rho_l\left(\frac{dR}{dt}\right)^2 + \frac{2\sigma}{R} \tag{22}$$

where, P_v is the vapor pressure of bubble, P_∞ is ambient pressure and t is the time.

The pressure difference can be related to the departing radius, R_d, using the static equilibrium since the radial acceleration and velocity are negligible close to the bubble departure (see Eq. (22)).

Therefore,

$$\Delta P = \frac{2\sigma}{R_d} \tag{23}$$

To effectively consider the results obtained from subcooled and superheated pool temperature conditions, we used a modified Jakob number, $Ja^* = (\rho_l C_{pl}\Delta T^*)/(\rho_v h_{fg})$, based on a new characteristic temperature, $T_c^* = \Delta T^*$, proposed by Kim et al. (2004).

$$T_c^* = f(T_{wall}, T_b, T_{sat}) = \beta(T_{wall} - T_{sat}) + (1-\beta)(T_b - T_{sat}) \tag{24}$$

where T_b is the bulk temperature and β is 0.7.

Then, the characteristic scales from Eq. (21) can be rewritten as

$$R_c = \frac{\sqrt{27}}{2} Ja\alpha \sqrt{\frac{\rho_l R_d}{\sigma}}, \quad t_c = \frac{9}{4} Ja\alpha \frac{\rho_l R_d}{\sigma} \tag{25a}$$

$$R_c^* = \frac{\sqrt{27}}{2} Ja^*\alpha \sqrt{\frac{\rho_l R_d}{\sigma}}, \quad t_c^* = \frac{9}{4} Ja^*\alpha \frac{\rho_l R_d}{\sigma} \tag{25b}$$

Finally, the dimensionless bubble radius (R^+ or R^*) and time (t^+ or t^*) can be expressed as

$$R^+ = \frac{R}{R_c}, \quad t^+ = \frac{t}{t_c} \tag{26a}$$

$$R^* = \frac{R}{R_c^*}, \quad t^* = \frac{t}{t_c^*} \tag{26b}$$

3.2. Results and discussion

The behavior of the bubble departure radius and time is plotted against the Jakob number in Fig. 3. The figure indicates that the departure radius and time were closely related to the Jakob number, as proposed in previous studies, regardless of the value of the Jakob number, fluid, pool temperature, or heating conditions.

For Jakob numbers higher than about 30, all except one set of data were obtained under sub-atmospheric pressures. Many previous and these author's studies for pool boiling were revealed that the transition from partial (isolated bubble) to fully-developed (bubble jet or column) nucleate boiling region could be occurred at about 30 of Jakob number ($\Delta T = T_{wall} - T_{sat}$: about 10) for water and about 32 for refrigerant R11 or R113 ($\Delta T = T_{wall} - T_{sat}$: about 25). The departure radius and time measured at sub-atmospheric pressure were usually greater than those measured at atmospheric pressures, as indicated in Fig. 3. It is well known that the growth behavior is one of the parameters that can affect the departure state. Under atmospheric and sub-atmospheric pressures, the departure characteristics are directly affected by the bubble growth behavior near the departure time. Nevertheless, it is difficult to demonstrate different bubble growth behaviors and the characteristics of the vapor pressure at departure experimentally and numerically.

As previous studies to analyze the departure behaviors, we performed the dimensional analysis. Fig. 4 shows the dimensionless departure radius and time, R_d^+ and t_d^+ (R_d^* and t_d^*), as functions of the Jakob number. The dimensionless bubble departure radius (R_d^+ or R_d^*) and time (t_d^+ or t_d^*) can be defined as

$$R_d^+ = \frac{R_d}{R_c}, \quad t_d^+ = \frac{t_d}{t_c} \tag{27a}$$

$$R_d^* = \frac{R_d}{R_c^*}, \quad t_d^* = \frac{t_d}{t_c^*} \tag{27b}$$

The figure clearly indicates the relationship between the dimensionless departure radius and time with Jakob number, even for different fluids, surface characteristics, heating conditions, and pool conditions. The dimensionless departure radius and time decreased with increasing Jakob number because the characteristic scales of the sub-atmospheric pressure were much greater than those of atmospheric pressure. The lines presented in the figure are the lines fitted for results obtained at only sub-atmospheric pressure. As shown in the figure, there are relatively large deviations between the results of the dimensionless bubble departure radius and time obtained at atmospheric pressure and the line. These deviations can be originated from the difference of the bubble growth behavior (growth rate) between atmospheric and sub-atmospheric pressure conditions, these phenomena were shown the effects of the liquid inertia on the departure behavior in some previous studies. Especially, Kiper (1971) showed that the dimensionless minimum departure radius is function of only Jakob number. To do that, he used the analytical method and the bubble growth equation as

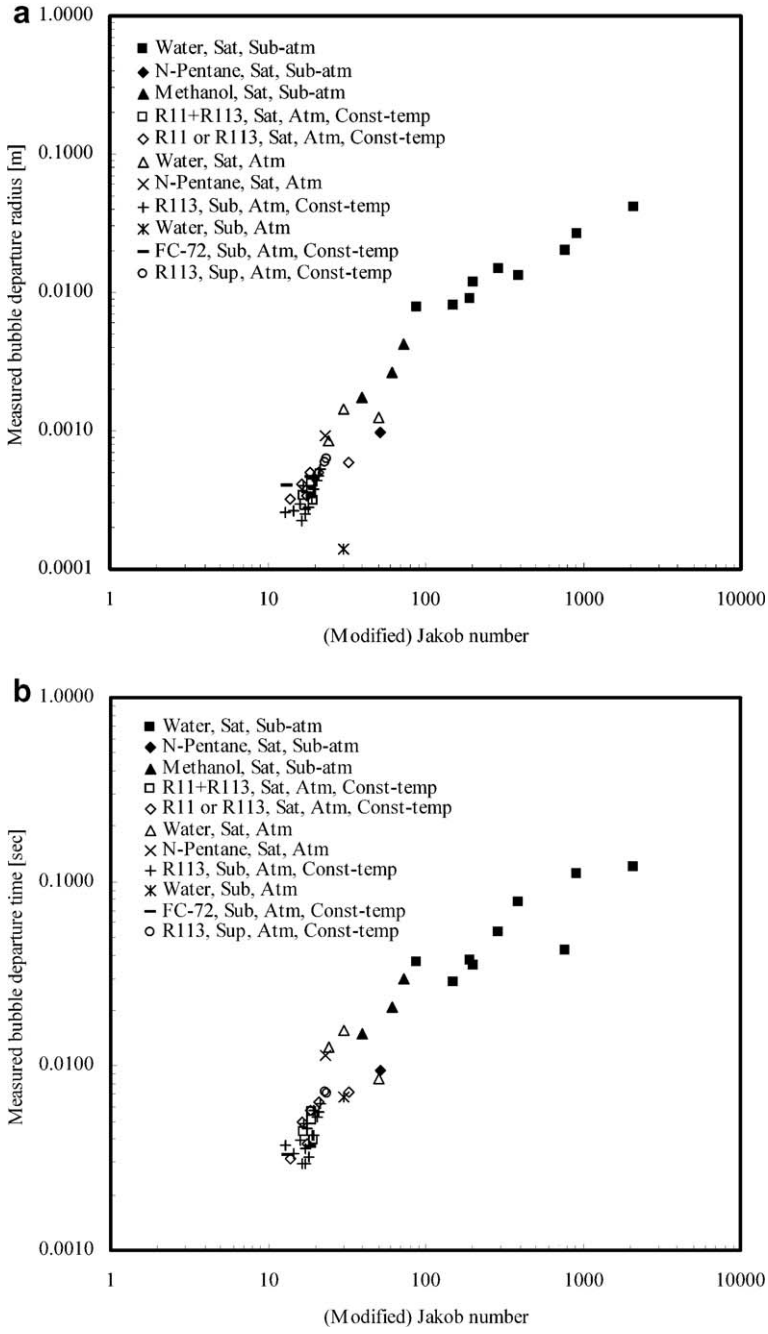

Fig. 3. Behavior of the bubble departure radius and time.

Eq. (28) to consider the liquid inertia regardless of low and high Jakob numbers. And, the constant C of the equation was function of thermal diffusivity and Jakob number.

$$R = Ct^{1/2} \tag{28}$$

But, Lee et al. (2003, 2004) showed that a bubble growth rate in thermal growth region near departure time was proportional to $(t^{+})^{1/5}$, which was slower than the growth rate proposed in previous analytical analyses at saturated and atmospheric conditions regardless of working fluids and heating conditions. And Kim et al.

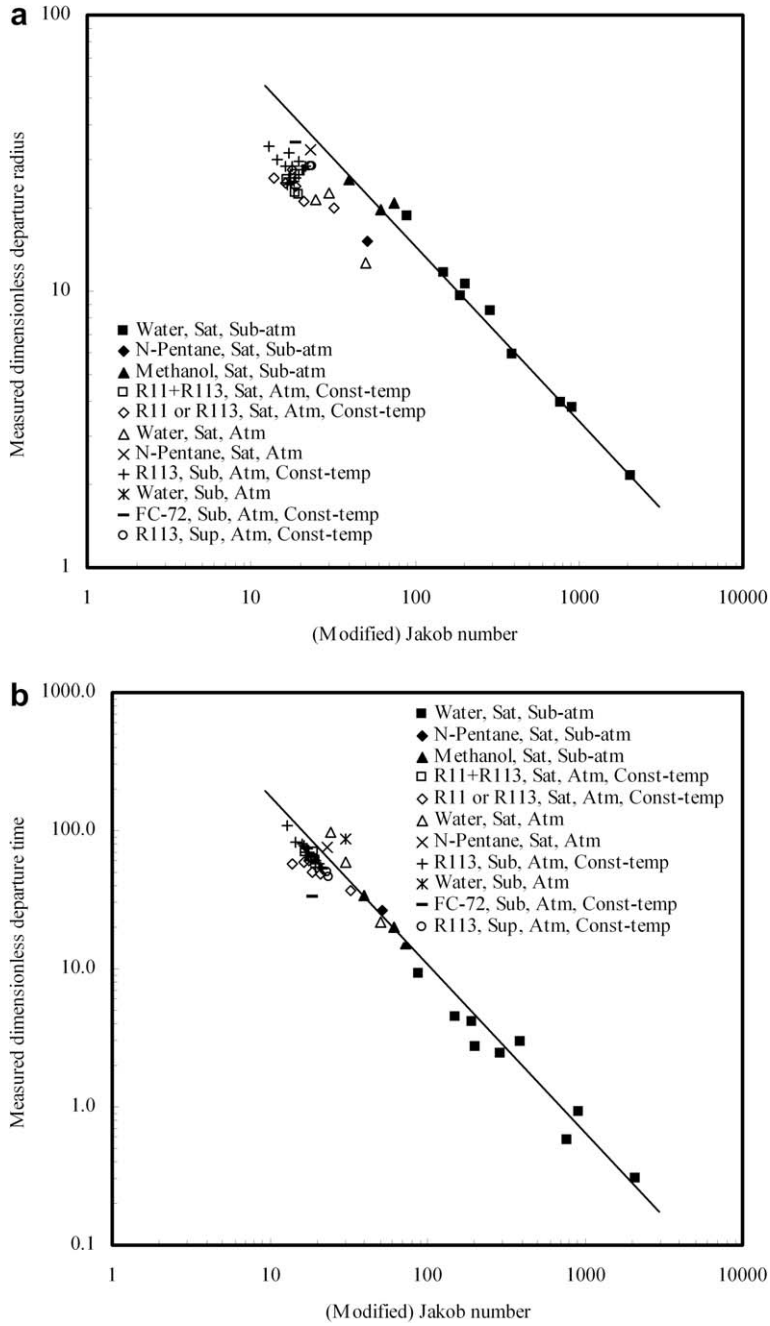

Fig. 4. Characteristics of the dimensionless departure radius and time.

(2004) also showed that a bubble growth rate at various pool temperature (subcooled, saturated, and superheated) and atmospheric conditions with the fixed wall temperature was proportional to $(t*)^{1/5}$ under constant temperature heating condition. Then again, to show the bubble growth rate at sub-atmospheric pressure, we performed the dimensional analysis using the characteristics scales proposed by Mikic et al. (1970) and presented as Fig. 5.

The result showed that a bubble growth rate at sub-atmospheric pressure conditions was proportional to between $(t^+)^{1/2}$ and $(t^+)^{1/3}$ near the departure time under constant heat flux heating condition regardless of

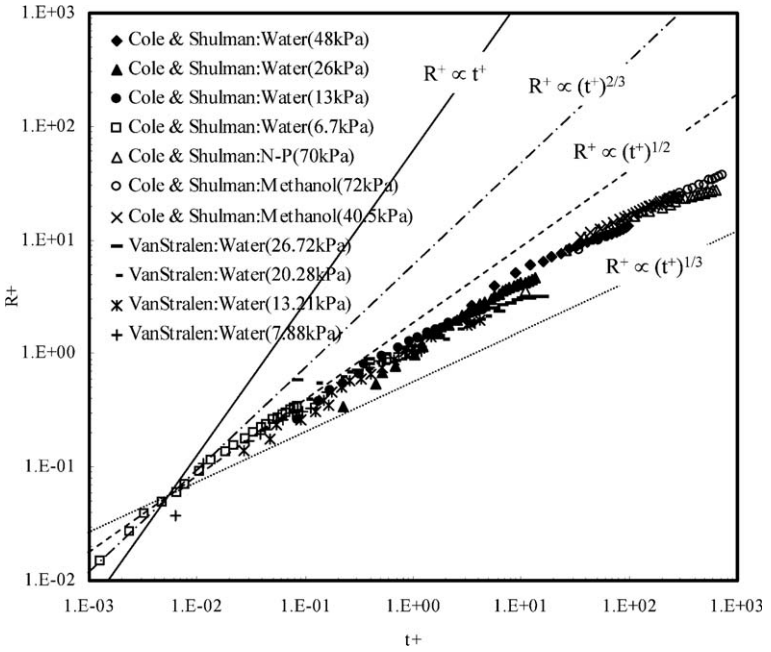

Fig. 5. The dimensionless bubble growth behavior at sub-atmospheric pressure.

working fluids and heating surface conditions. The growth rate at sub-atmospheric pressure is very higher than that at atmospheric pressure. The growth rate difference can be firstly estimated from the initial pressure potential difference

$$\Delta P^{+} = \frac{P_{\mathrm{v}}(T_{\mathrm{wall}}) - P_{\mathrm{sys}}}{P_{\mathrm{sys}}} \tag{29}$$

as illustrated in Fig. 6(a).

The initial vapor pressure was calculated as a function of the wall temperature. The pressure potential of higher Jakob numbers was relatively higher than that of atmospheric pressure. In addition, higher Jakob number for sub-atmospheric pressures corresponded to very low vapor densities, as shown Fig. 6(b), due to the density ratio

$$\rho^{+} = \frac{\rho_{\mathrm{v}}}{\rho_{\mathrm{l}}} \tag{30}$$

Even if the mass of liquid evaporated in the interface between bubble and the surrounding liquid is same, the volume change of bubble will be relatively increased owing to high specific volume. So, the bubble growth rate is the ratio of the volume change of bubble, or the evaporation rate of the bubble, to time change, that will be depended on the thermal boundary layer thickness around the bubble and the temperature gradient in the bubble interface. At sub-atmospheric pressure, the growth rate could be higher due to the relatively high wall superheat and the difference of thermodynamic property (high Jakob number) than that of atmospheric pressure. So, the liquid inertia effect originated from the different growth rates can make different departure behaviors for each pressure conditions. As proposed by Lee et al. (2003, 2004), we also found that the dimensionless departure radius (R_{d}^{+} or R_{d}^{*}) was approximately 25, and the dimensionless departure time (t_{d}^{+} or t_{d}^{*}) was approximately 60, regardless of the boundary conditions, pool temperatures, or working fluids used for nucleate pool boiling experiments with atmospheric pressure except for the result of Fontana (1972). Using the values of the dimensionless departure radius and time, the dimensional departure radius and time can be predicted as follows:

$$R_d^+ = \frac{R_d}{\frac{\sqrt{27}}{2} Ja\alpha \sqrt{\frac{\rho_l R_d}{\sigma}}} = 25$$
$$t_d^+ = \frac{t_d}{\frac{9}{4} Ja\alpha \frac{\rho_l R_d}{\sigma}} = 60 \quad (31)$$

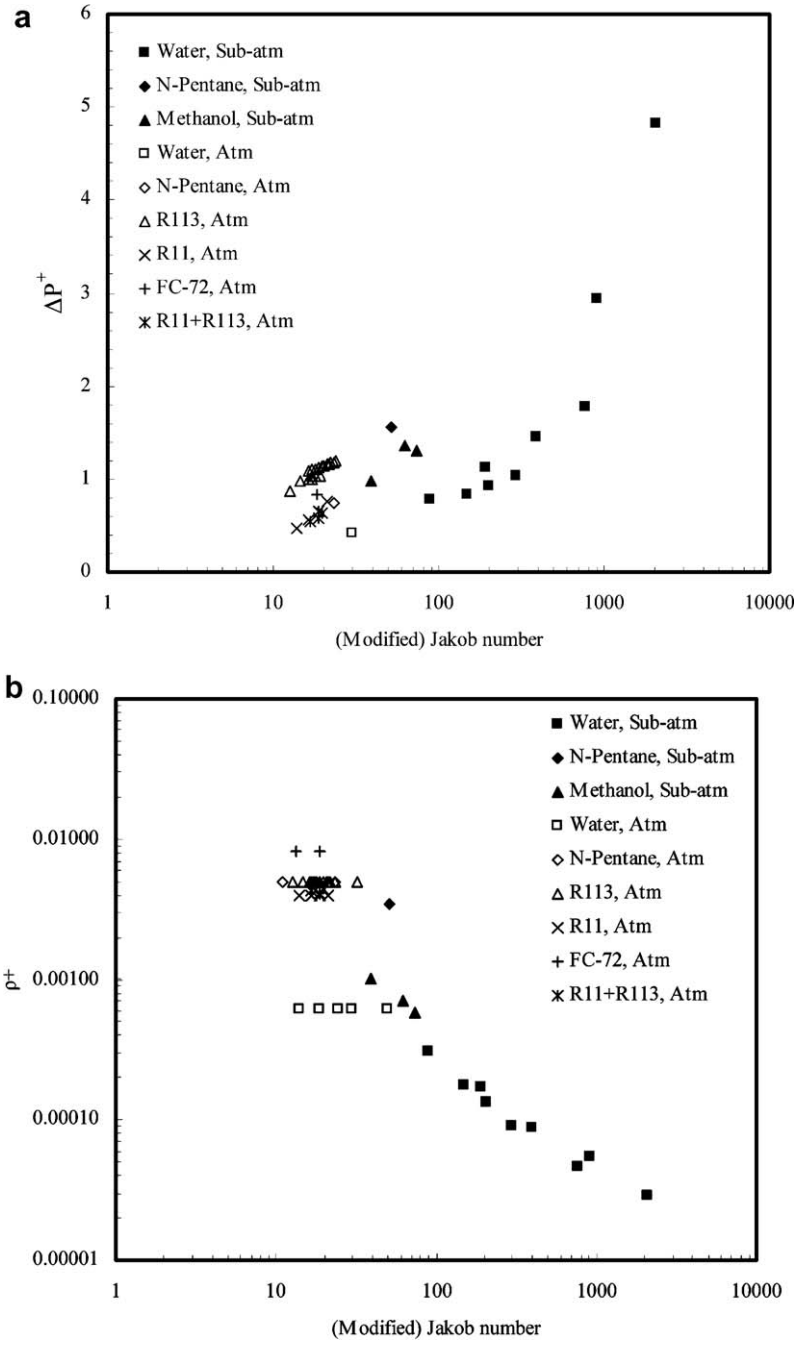

Fig. 6. Dimensionless initial pressure potential and vapor density.

$$R_{\mathrm{d}} = \left[25\frac{\sqrt{27}}{2}Ja\alpha\sqrt{\frac{\rho_{\mathrm{l}}}{\sigma}}\right]^2$$
$$t_{\mathrm{d}} = 60\frac{9}{4}Ja\alpha\frac{\rho_{\mathrm{l}}R_{\mathrm{d}}}{\sigma} \tag{32}$$

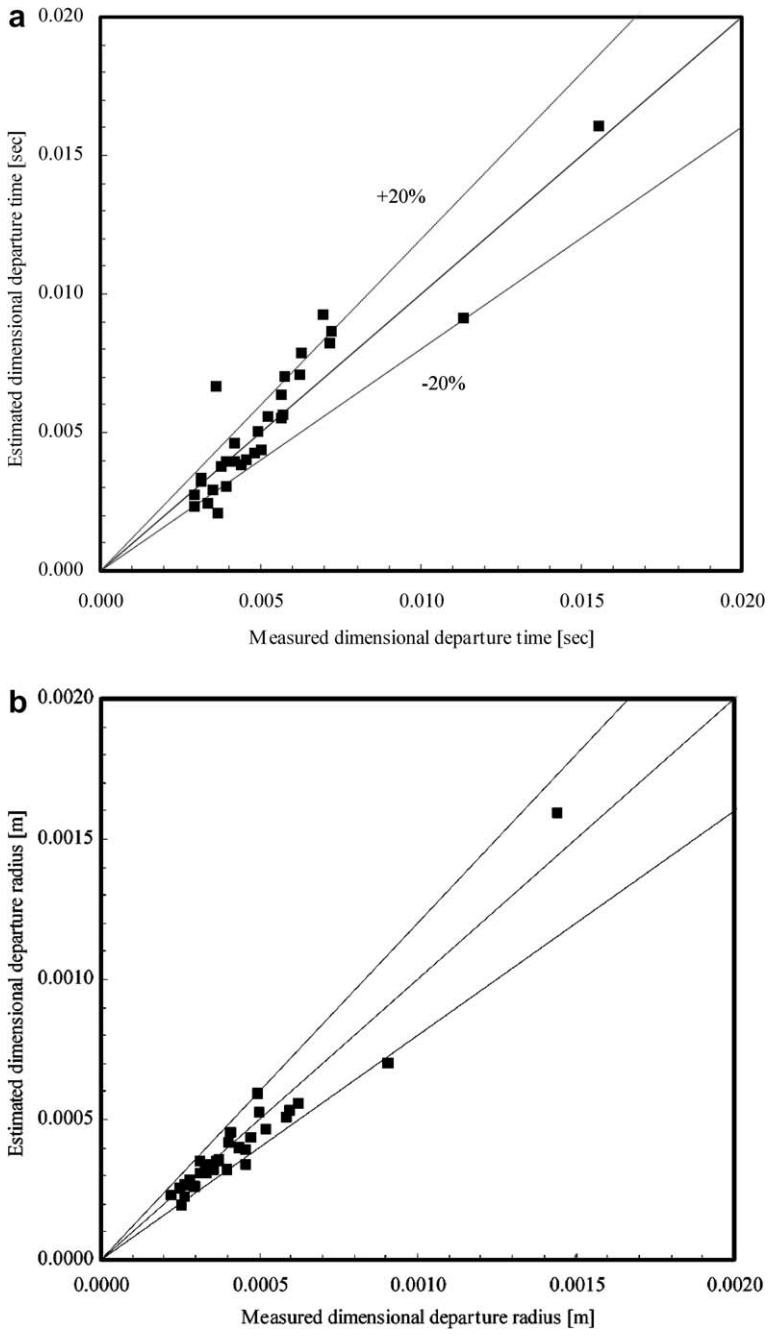

Fig. 7. Comparison of the estimated and experimental dimensional departure radius and time at atmospheric pressure.

And, fitted the dimensionless departure radius (R_d^+ or R_d^*) and time (t_d^+ or t_d^*) as function of Jakob number (Ja or Ja^*) regardless of the boundary conditions, pool temperatures, or working fluids used for nucleate pool boiling experiments with sub-atmospheric pressure and presented the equation as follows:

$$R_d^+ = 244.398 Ja^{-0.612}$$
$$t_d^+ = 2369.97 Ja^{-1.194} \quad (33)$$

Fig. 7 compares the dimensional departure radius and time estimated from the proposed relations, Eq. (32), with the experimental results obtained under atmospheric pressure. The dimensional departure radius and time obtained from Eq. (32) proposed for atmospheric condition in this study were well predicted within a ±20% error. And the departure radius estimated using the proposed correlations, Eq. (32), at atmospheric was in better agreement with measured data when compared with the result obtained from previous correlations, as shown in Fig. 8.

Fig. 9 compares the dimensionless departure radius and time obtained using the proposed correlations, Eq. (33), with experimental results for sub-atmospheric pressure conditions. As was the case for atmospheric pressure conditions, the departure radius and time were also predicted with ±20% error, and the proposed correlations were in better agreement with measured data when compared with the result from the correlations proposed in previous studies (see Fig. 10).

The preceding results show that we can obtain a relationship for the departure behavior of bubbles during nucleate pool boiling under a range of conditions, including constant heat flux and temperature pool conditions; subcooled, saturated, and superheated thermodynamic conditions; and atmospheric and sub-atmospheric pressure conditions. Based on these results, we propose the following relationship between the Jakob and Bond numbers for sub-atmospheric pressure condition like as presented at previous studies:

$$Bo^{1/2} = 0.1649 Ja^{0.7} \quad (34)$$

as illustrated in Fig. 11. The square root of the Bond number was proportional to the Jakob number raised to the power of 0.7, which differs from previous correlations, such as those proposed by Ruckenstein (1963) and Cole (1967).

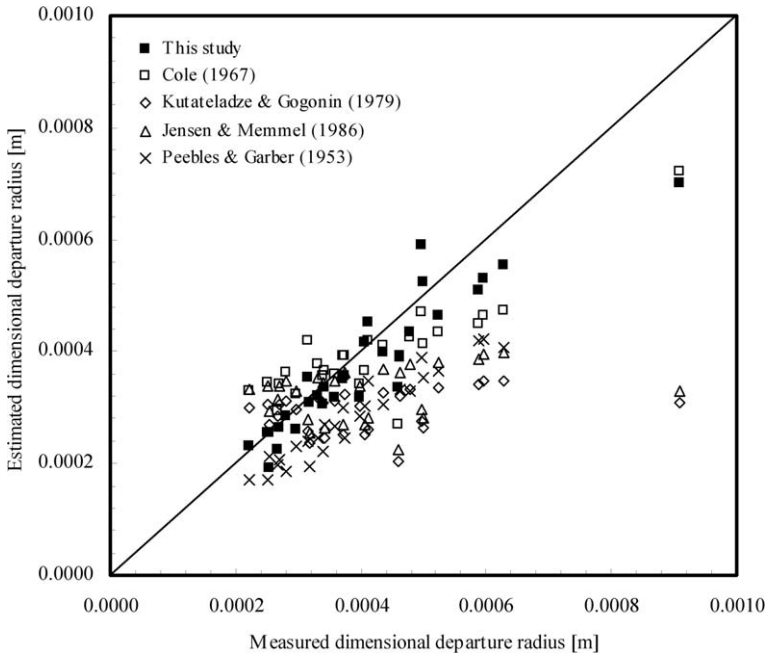

Fig. 8. Comparison of the correlations obtained in this study and previous studies at atmospheric pressure.

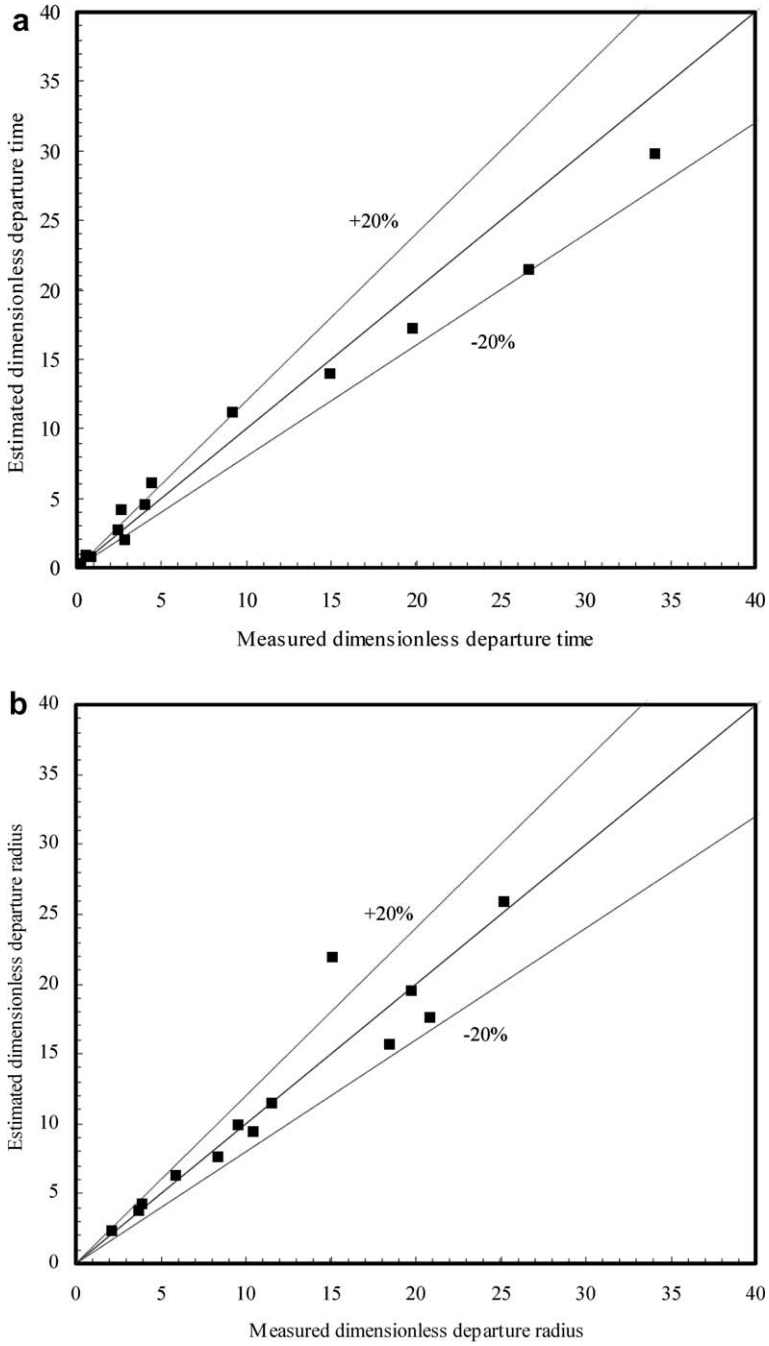

Fig. 9. Comparison of the estimated and experimental dimensionless departure radius and time at sub-atmospheric pressure.

4. Conclusions

A quantitative analysis of bubble departures during nucleate pool boiling was performed using the characteristic bubble radius and time scales we proposed in a previous study. Dimensionless scales were obtained from experimental data reported in many studies and include partial nucleate pool boiling data with constant heat flux and temperature conditions at atmospheric and sub-atmospheric pressures, as well as data obtained at subcooled, saturated, and superheated pool conditions.

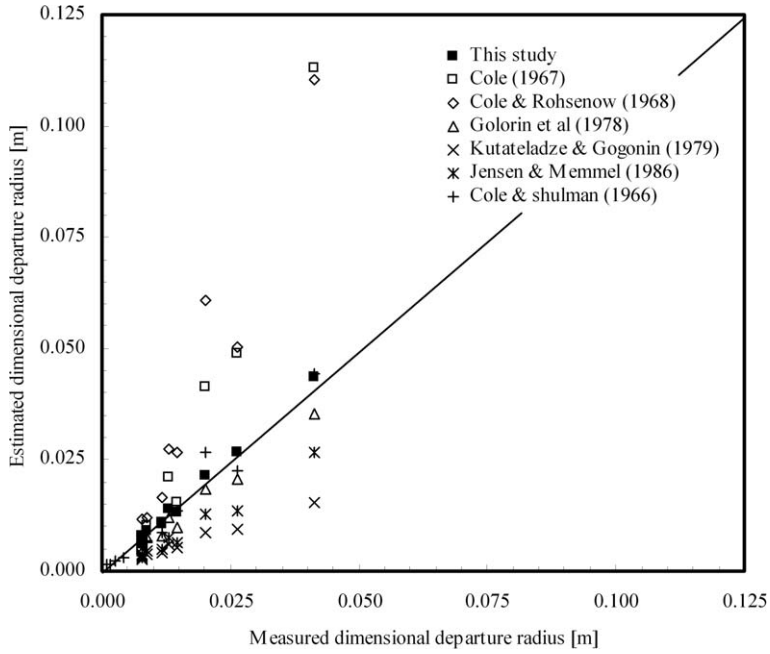

Fig. 10. Comparison of the correlations obtained in this study and previous studies at sub-atmospheric pressure.

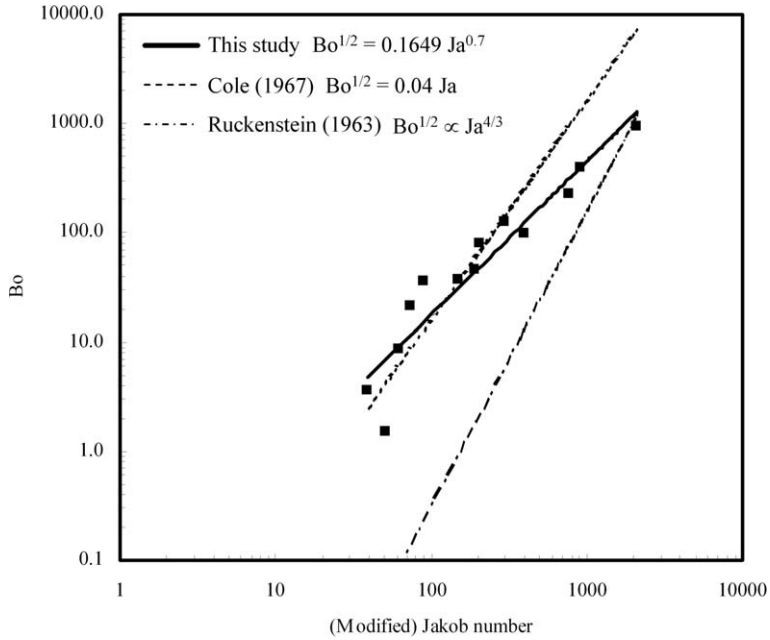

Fig. 11. Relationship between the Jakob and Bond numbers at sub-atmospheric pressure.

The departure characteristics of bubble were classified between atmospheric and sub-atmospheric pressure, showed different behaviors between low and high Jakob number. Typically as known, the classification was originated from the difference growth rate near the departure time.

From the results under atmospheric pressure, it was shown that the dimensionless departure radius and time scales were about 25 and 60 regardless of the surface characteristics, the heating conditions, the working

fluids, and pool temperatures, respectively. For higher Jakob number, the close relations between the departure radius and time and Jakob number were shown, as like the results proposed by the previous studies. And the square root of Bond number was proportional to the power of 0.7 of Jakob number, little different from the previous correlations.

Finally, the relationships for low and high Jakob numbers proposed in this study could well predict and describe the departure behaviors of bubble on the heating surface with $\pm 20\%$ error.

Acknowledgments

This work was supported by the Ministry of Science and Technology of Korea through the National Research Laboratory program. The authors thank the previous researchers that analyzed bubble departure behavior during nucleate pool boiling and obtained the results presented in Table 2.

References

Borinshansky, V.M., Fokin, F.S., 1963. Heat Transfer and Hydrodynamics in Steam Generators. Trudy TsKTI 62, 1.

Carey, V.P., 1992. Liquid-Vapor Phase-Change Phenomena: An Introduction to the Thermophysics of Vaporization and Condensation Processes in Heat Transfer Equipment. Taylor & Francis, pp. 206–211.

Cole, R., 1960. Photographic study of boiling in the region of critical heat flux. AIChE J. 6, 533–542.

Cole, R., 1967. Frequency and departure diameter at sub-atmospheric pressures. AIChE J. 13, 779–783.

Cole, R., Rohsenow, W.M., 1968. Correlation of bubble departure diameters for boiling of saturated liquids. Chem. Eng. Prog. Symp. Ser. 65, 211–213.

Cole, R., Shulman, H.L., 1966a. Bubble growth rates at high Jakob numbers. Int. J. Heat Mass Transf. 9, 1377–1390.

Cole, R., Shulman, H.L., 1966b. Bubble departure diameters at subatmospheric pressures. Chem. Eng. Prog. Symp. Ser. 62, 6–16.

Coleman, W.H., Steele, W.G., 1989. Experimentation and Uncertainty Analysis for Engineers. John Wiley & Sons.

Fontana, D.M., 1972. Simultaneous measurement of bubble growth rate and thermal flux from the heating wall to the boiling fluid near the nucleation Site. Int. J. Heat Mass Transf. 15, 707–714.

Fritz, W., 1935. Berechnung des Maximalvolume von Dampfblasen. Phys. Z. 36, 379–388.

Golorin, V.S., Kol'chugin, B.A., Zakharova, E.A., 1978. Investigation of the mechanism of nucleate boiling of ethyl alcohol and benzene by means of high-speed motion-picture photography. Heat Transfer Sov. Res. 10, 79–98.

Han, C.H., Griffith, P., 1965. The mechanism of heat transfer in nucleate pool boiling—Part I. Bubble initiation, growth and departure. Int. J. Heat Mass Transf. 8, 887–904.

Ivey, H.J., 1967. Relationships between bubble frequency, departure diameter an rise velocity in nucleate boiling. Int. J. Heat Mass Transf. 10, 1023–1040.

Jakob, M., Fritz, W., 1931. Frosh. Geb. Ingenieurwes 2, 434.

Jensen, M.K., Memmel, G.J., 1986. Evaluation of bubble departure diameter correlations. Prog. Eighth Int. Heat Transf. Conf. 4, 1907–1912.

Kim, J., Benton, J.F., Wisniewski, D., 2002. Pool boiling heat transfer on small heaters: effect of gravity and subcooling. Int. J. Heat Mass Transf. 45, 3919–3932.

Kim, J., Oh, B.D., Kim, M.H., 2004. Effect of various pool temperature conditions on partial nucleate boiling. ICMF-2004. Yokohama. Paper No. 293.

Kiper, A.M., 1971. Minimum bubble departure diameter in nucleate pool boiling. Int. J. Heat Mass Transf. 14, 931–937.

Kutateladze, S.S., Gogonin, I.I., 1979. Growth rate and detachment diameter of a vapor bubble in free convection boiling of a saturated liquids. High Temp. 17, 667–671.

Lee, H.C., Oh, B.D., Bae, S.W., Kim, M.H., 2003. Single bubble growth in saturated pool boiling on a constant wall temperature surface. Int. J. Multiphase Flow 29, 1857–1874.

Lee, H.C., Kim, J., Oh, B.D., Kim, M.H., 2004. Single bubble growth in saturated pool boiling of binary mixtures. Int. J. Multiphase Flow 30, 697–710.

Mikic, B.B., Rohsenow, W.M., 1969. Bubble growth rates in non-uniform temperature field. Prog. Heat Mass Transf. II, 283–293.

Mikic, B.B., Rohsenow, W.M., Griffith, P., 1970. On bubble growth rates. Int. J. Heat Mass Transf. 13, 657–666.

Peebles, F.N., Garber, H.J., 1953. Studies on motion of gas bubbles in liquids. Chem. Eng. Prog. 49, 88–97.

Ruckenstein, E., 1963. Physical model for nucleate boiling heat transfer from a horizontal surface. Bul. Institutului Politech. Bucaresti. 33, 79–88.

Rule, T.D., Kim, J., 1999. Heat transfer behavior on small horizontal heaters during pool boiling. J. Heat Transf. 121, 386–393.

Rule, T.D., Kim, J., Kalkur, T.S., 1998. Design, construction and qualification of a microscale heater array for use in boiling heat transfer. NASA/CR-1998-207407.

Staniszewski, B.E., 1959. Nucleate boiling bubble growth and departure. M.I.T. DSR Project No. 7-7673, Technical Report No. 16.

van Stralen, S.J.D., Sohal, M.S., Cole, R., Sluyter, W.M., 1975. Bubble growth rates in nucleate boiling of water at subatmospheric pressures. Int. J. Heat Mass Transf. 18, 655–669.

Zuber, N., 1959. Hydrodynamic aspects of boiling heat transfer. US AEC report AECU 4439, June.

Zuber, N., 1961. The dynamics of vapor bubbles in nonuniform temperature fields. Int. J. Heat Mass Transf. 2, 83–98.

Zuber, N., 1963. Nucleate boiling the region of isolated bubbles similarity with natural convection. Int. J. Heat Mass Transf. 6, 53–65.